Radiation characteristics of low and high clouds in different oceanic regions observed by CERES and MODIS

BING LIN*†, PATRICK MINNIS†, TAI-FANG FAN‡,
YONGXIANG HU†, AND WENBO SUN‡
†Climate Sciences, NASA Langley Research Center
Hampton, VA 23681

‡SSAI, One Enterprise Parkway
Hampton, VA 23666

Submitted to the Int. J. Remote Sens.
Revised April, 2009
Accepted April, 2009

*Corresponding author's address: Dr. Bing Lin, MS 420, NASA Langley Research Center, Hampton, VA 23681-2199; email: bing.lin@nasa.gov; phone: 757-864-9823; fax: 757-864-7996.

Radiative properties measured by the Clouds and the Earth's Radiant Energy System and Moderate-resolution Imaging Spectroradiometer on the *Aqua* spacecraft are evaluated for the same types of clouds in selected areas. Individual measurements are statistically analyzed to take an advantage of both gridded and individual cloud characteristics. The seasonal variations of radiative fluxes for the same types of clouds from different areas are remarkably similar. Although cloud liquid or ice water paths vary considerably for the same types of clouds, their statistical distributions are very stable for different periods and areas, suggesting that the regional differences in dynamics and thermodynamics primarily cause changes in the cloud frequency or coverage and only secondarily in the cloud macrophysical characteristics such as ice or liquid water path. These results establish a systematic approach of observations for testing modeled cloud statistics and for improving cloud model parameterizations.

Key words

Satellite measurement, liquid and ice water path, cloud cover, cloud radiation

1. Introduction

During the last 2-3 decades, the parameterization and representation of cloud properties have been a focus of global climate model (GCM) studies. Yet, significant problems remain for characterizing clouds accurately in the models, and subsequently the changes in clouds and their feedbacks with changing climate are highly uncertain. Cloud cover and its vertical distributions determined from GCMs for the current climate differ significantly from the observations despite relatively large uncertainties in the latter (*Zhang et al.* 2005). The cloud ice water paths (IWP) derived by GCMs are highly model dependent and differ markedly from the observations in many cases (*Waliser et al.*2009). Some of these problems are caused by theoretical and numerical modeling shortcomings, and the others are due to uncertainties in the observations. Much additional work is needed to better understand the observations and to develop more accurate cloud parameterizations, especially for particular cloud types.

Tropical deep convective systems not only generate heavy precipitation and transport moisture to the upper troposphere but also have crucial effects on atmospheric radiation due to their large horizontal and vertical extents. Large amounts of marine boundary-layer clouds form under the subsidence of the Hadley and Walker circulations and the temperature inversion associated with the top of the boundary layer. Because of the preferred large-scale dynamics and local thermodynamics, marine boundary-layer clouds, in particular stratus and stratocumulus, impose a persistent negative radiative forcing, or cooling, that affects the tropical atmospheric circulation patterns. The radiative properties of these clouds, such as optical depth (τ), liquid water path (LWP), IWP, cloud temperature (Tc), effective cloud droplet radius (Re) and ice crystal diameter (De), shortwave (SW) and longwave (LW) fluxes, and cloud areal coverage (Ac), range from very small to extremely large values. Current cloud parameterizations in GCMs and, even, in cloud resolving models cannot simulate all of the detailed physical processes that operate inside clouds and within the boundary layer.

Most knowledge of clouds and their feedbacks has been obtained from observations of cloud water amount (or its closely related variable, optical depth), particle size, and associated radiation. Satellite and ground-based measurements revealed that the change in cloud thickness is the primary cause of the LWP variation with temperature (Tselioudis *et al.* 1992, Del Genio and Wolf, 2000, Lin et al. 2003). For high clouds, although there were significant differences in the interpretations of satellite observations during the last decade or so (e.g., Ramanathan and

Collins 1991, Fu *et al.* 1992, Hartmann and Michelsen 1993, 2002, Lindzen *et al.* 2001) studies based on the latest satellite observations (Lin *et al.* 2002, Del Genio and Kovari 2002, Del Genio *et al.* 2005, Rapp *et al*. 2005, Su *et al*. 2006, Lin *et al*. 2006, 2007) appear to be converging.

A typical approach for characterizing large-scale cloud properties is to compute averages of gridded satellite measurements (e.g., Tselioudis *et al.* 1992, Cess *et al.* 2001). The advantage of this approach is that the observed averages can be directly used to compare with the results from GCMs due to the similarities in climate regimes and large-scale dynamical forcings. Even the grid sizes and temporal resolutions are generally similar. Also, the computational resources and requirements in data processing are normally manageable for most modeling institutes. A disadvantage is that different types of clouds are likely mixed together in the gridded data, especially for monthly or longer time scale means. The detailed physical properties associated with individual cloud types, thus, may not be obtained. To overcome this problem, another approach that analyzes individual cloud types, systems, and objects is also frequently used for satellite observations. Such approach can trace the back trajectory of individual clouds and evaluate the life cycle of these clouds (Machado *et al.* 1998, Luo and Rossow 2004). The radiative properties of huge cloud systems and the influence of environmental conditions on these systems can also be specifically identified (Lin *et al.* 2006, 2007). Furthermore, the statistics that characterize particular cloud objects are observed (Machado *et al.* 1998, Xu *et al.* 2005, 2008, Eitzen *et al.* 2008). Because of the complexity in identifying individual cloud systems and the satellite data availability, there is generally no long-term (e.g., interannual) statistical analysis in cloud objects (Xu *et al.* 2005, 2008, Eitzen *et al.* 2008). Although this approach targets the statistics and physical processes of cloud systems, GCMs may not be capable of replicating the observations of individual clouds and generally cannot trace individual cloud systems due to spatial scale differences in the observational analysis and model simulations. The computational power requirements for this approach are also very high.

Recently, there are significant progresses in identifying cloud regimes using cluster analysis from gridded statistics (Jakob and Tselioudis 2003, Rossow et al. 2005, Jakob et al. 2005). These studies construct 2-dimensional histograms of cloud top pressure and optical depth from satellite observations for individual $1° \times 1°$ grid boxes and identify regional cloud types and meteorological conditions for these regional grids. The basic relationships between cloud properties and weather dynamics, such as ascent and descent, have been established and used for

GCM and satellite cloud comparisons (e.g., Bony et al. 2006). This study also takes advantage of both gridded and individual cloud system analyses, and evaluates same types of clouds occurring at different geographical locations. We will evaluate the consistencies and differences in the characteristics of cloud systems for different times and places with the goal of providing modelers with a basic tool for modeling and assessing observed and simulated clouds. The potential analysis regions are first identified from the gridded annual mean satellite data based on clouds belonging to similar climate regimes. Within these identified regions, the statistical characteristics for each cloud type are computed using radiative fluxes from each Clouds and the Earth's Radiant Energy System (CERES, Wielicki *et al.* (1996)) scanner pixel and cloud properties derived from matched Moderate-resolution Imaging Spectroradiometer (MODIS) measurements. The next section introduces the data sets and analysis methods, and Section 3 presents the observational results for the different cloud types. The similarity and difference among the clouds from different regions are discussed. Section 4 summarizes the findings of this study.

2. Data analysis

The measurements used here were taken by instruments on the *Aqua* satellite from January 2003 through December 2005. During this time period, there were no significant global or tropical scale climatological anomalies such as El Nino and La Nina. Thus, the satellite observed results should represent clouds in fairly averaged climate conditions. This time period is also constrained by the availability of the CERES single scanner footprint (SSF) product that includes the temporally and spatially matched CERES and MODIS measurements.

CERES measures top-of-atmosphere (TOA) broadband SW and LW radiances directly at a spatial resolution of about 20 km, and estimates both TOA and surface SW, LW and net radiative fluxes based on the radiance measurements and the merged MODIS-based cloud and aerosol information. By merging the cloud and radiance measurements, CERES is able to reduce the TOA SW and LW radiative fluxes for specific cloud (and clear) types down to instantaneous errors of ~13 and ~4.3 Wm^{-2}, respectively, values at least a factor of two smaller than those from the Earth Radiation Budget Experiment (ERBE, Barkstrom *et al.* (1989)). The errors in averaged values are significantly smaller. For surface radiative fluxes, the estimated error uncertainties in regional monthly means are about 10 Wm^{-2} (Lin *et al*. 2008).

The cloud properties derived by CERES mission are based on the *Aqua* MODIS 1-km visible (VIS, 0.64 μm), solar infrared (3.8 μm), infrared (IR, 10.8 μm), and split-window (12.0 μm) measurements after first classifying each pixel as clear or cloudy as discussed in Minnis *et al.* (2008). For the cloudy pixels, the effective cloud temperature and height, cloud thermodynamic phase (P_{wi}), and the other microphysical properties mentioned earlier are retrieved using updates of the VIS-IR-Solar-IR-Split-window technique (VISST) during the day and the Solar-infrared-IR-Split-window technique (SIST) at night (Minnis *et al.* 1995). The detection threshold for thin clouds of the VISST and SSIT technique is about optical depth 0.3. For this study, the retrievals of cloud LWP, IWP and optical depth are only available for daytime MODIS measurements taken near 13:30 local time. The radiative fluxes shown later represent the atmospheric diabetic heating at the time of satellite overpasses. Other cloud properties, such as cloud top temperature and pressure, are estimated from both day- and night-time MODIS measurements. After the cloud retrieval for each MODIS pixel, all cloud properties from the MODIS data are convolved into the corresponding CERES footprint, minimizing collocation errors.

The *Aqua* Edition-1 CERES SSF data are used to identify certain cloud types and to select the typical regions where those clouds are most common. Initial comparisons with radar and lidar data indicate that the marine boundary-layer cloud heights retrieved by CERES are, on average, ~0.3 km greater than those derived from lidar measurements taken by the Cloud and Aerosol Lidar (Sun-Mack *et al.* 2007). While direct validation of the low-cloud optical properties over ocean has not yet been performed, comparisons with retrievals using surface-based radar and radiometer data over land indicate good agreement between the satellite and surface retrievals of Re, τ, and LWP (Dong *et al.* 2008). The optical properties for optically thin cirrus clouds are also in good agreement with radar and lidar retrievals of De, τ, and IWP (Mace *et al.* 2005, Chiriaco *et al.* 2007), and the magnitude and distribution of IWP are very close to those derived from the CloudSat cloud radar (Waliser *et al.* 2008). However, the top heights of optically thin cirrus are typically underestimated by 1 or 2 km by the MODIS retrievals, and very thin cirrus clouds, typically with $\tau < 0.3$, are not detected (Mace *et al.* 2005, Chiriaco *et al.* 2007, Sun-Mack *et al.* 2007). Although the detection and cloud top height estimation of thin cirrus clouds may be significantly improved by applying CO_2 slicing technique to MODIS data (Chang and Li 2005a), current CERES operational cloud retrieval technique for MODIS and other

satellite sensors has not implemented the CO_2 method, which may result in overestimations of cloud amounts of middle level clouds (Chang and Li 2005b). To avoid mischaracterization of middle clouds, this study only discusses low and high clouds identified in the CERES cloud product. For this study, low and high clouds are defined as satellites pixels having cloud top pressure greater than 680 hPa and less than 440 hPa, respectively.

To select the low and high cloud regions for this study, the annual distributions of these kinds of clouds are examined first. To minimize background variability effects on the retrievals only oceanic clouds are considered. Figure 1 shows the annual mean high (upper panel) and low (lower panel) cloud cover for 2005 obtained from the CERES SSF product. Corresponding to this figure, some typical high and low cloud areas are highlighted and labeled in Figure 2. All climatologically stormy areas are evident as regions with a large (> 18%) mean fraction of high cloud cover. For example, middle latitude storms are highly concentrated on the Atlantic and Pacific storm tracks (areas labeled 1-4 in the upper panel of Figure 2). Some places within these regions even have annual mean high cloud fractions greater than 30%. The areas with the greatest high cloud cover are the tropical western Pacific (TWP) and eastern India Ocean (i.e., areas 5, 6, 8, 9) with peak values up to ~50%. The 9 high-cloud areas include 4 mid-latitude storm track regions (1 each in the North Atlantic, South Atlantic, North Pacific, and South Pacific), and 5 tropical deep convective regions (eastern Pacific and Atlantic intertropical convergence zones (ITCZ), northern TWP, southern TWP and South Pacific Convergence Zone (SPCZ), northern and southern tropical Indian Ocean). For low clouds, persistent marine stratus and stratocumulus clouds occurring more than 45% of the time year-round are found in the upwelling oceanic areas west of the southern Africa, Australia, California, and South America (labeled as 1-4 in the lower panel of Figure 2). Because of both large spatial coverage and significant optical thickness, these clouds comprise one of the dominant factors that influence the global radiation budget. Note that the low cloud amounts in Figure 1 are likely smaller than those seen elsewhere because the *Aqua* daytime overpass is near the time of minimum cloudiness in marine stratus areas.

To compute the cloud properties within each region, only those $1° \times 1°$ grid boxes having annual mean cloud amounts greater than 18% and 45% were used for high and low clouds, respectively, to ensure some uniformity across regions. Because of large-scale atmospheric waves and the intermittent nature of deep convection, mesoscale convective clouds, frontal

systems and even stratus clouds generally do not continuously stay in each grid box. The actual cloud properties analyzed for those 1° × 1° grid boxes were, thus, the statistical values from individual CERES pixels satisfying the low and high cloud definitions mentioned previously, i.e., they were obtained from instantaneous satellite observations for each type of the clouds in the selected grids. This way would ensure that large-scale conditions were favorable for the selected cloud types even in local and short-time scales. To obtain their statistically-stable distributions, these individual cloud properties were cumulated in monthly and longer time scales. The purpose of our multiple scale cloud analysis process is to pick up the areas that have persistently favorable climate conditions for the analyzed clouds to grow (annual scale), to catch up with seasonal variations in the areas for the clouds (monthly scale), and to determine weather conditions for the clouds to develop at the observational moment and individual location. From this and previous considerations, it can be seen that the high or low cloud characteristics considered here conserve the cloud features over a wide range of scales from individual satellite footprints to cumulative quantities of a typical grid box up to the entire selected climatological area at monthly or longer time scales.

3. Results and discussion

Figures 3 and 4 show the time series of monthly mean cloud cover during the study period for the selected areas. For the storm track areas (Figure 3, upper panel), mean high cloud cover generally varies from 15 to 35 % occurring more frequently during the hemispheric spring and summer seasons. In the marine stratus regimes, the low cloud amounts (Figure 3, lower panel) are generally high, mostly greater than about 50%. These results are consistent with the surface-based climatology (Klein and Hartmann 1993), showing similar seasonal variations and less stratus west of Australia. The strong annual cycles in the eastern Pacific and southeastern Atlantic areas may be related to large seasonal zonal shifts of subsidence in the eastern subtropical Pacific and Atlantic and their associated ocean upwelling variations. Weaker large-scale forcing off the west coast of Australia than in the other three regions produces generally weaker low-level stability and, hence, less persistent boundary-layer clouds (Klein and Hartmann 1993). The seasonal variability of cloud cover in the southeastern Atlantic (area 1, black) appears to be comparable to those in the eastern Pacific areas although the cloud cover may be a little less than in the other areas. The minimum stratus coverage occurs around the beginning of

each year regardless of hemisphere, suggesting that the forcing mechanisms differ between the hemispheres.

The tropical high cloud amounts (Figure 4), mainly from mesoscale convective systems (Lin *et al.* 2006), in the northern tropical Indian Ocean along the ITCZ (area 9, upper panel) have a larger annual cycle than those in the southern tropical Indian Ocean (area 6) owing to the contrast between the Indian subcontinent and the sea as well as the Indian monsoon. The high clouds in the ITCZ over the northern TWP (area 8) and SPCZ (area 5) have similar areal coverage, while their annual variabilities are 6 months out of phase due to the seasonal shifts in solar radiation. The cirrus and convective clouds in the tropical eastern Pacific and Atlantic (area 7) ITCZs generally are less frequent than those in the northern TWP and the India Ocean and have smaller seasonal changes in areal coverage. For the ITCZ across the globe (areas 7, 8, and 9 combined, lower panel, hereafter also called ITCZ), the annual cycle of high cloud cover is dominated by the northern TWP and India Ocean, at least, for the 'normal' climate years analyzed here. During 2003-2005, the ITCZ has not changed from its normal conditions greatly and no double ITCZs were observed. An El Nino or La Nina climate would significantly shift the TWP convergence zones to the central Pacific and cause huge changes in high cloud cover in the tropical eastern Pacific and Atlantic (area 7) (Cess *et al*. 2001).

The high clouds in the Indian Ocean (areas 6 + 9) appear as frequently as those in the tropical western Pacific (areas 5 + 8) since the areas of both northern tropical western Pacific (area 5) and SPCZ (area 8) extend to the middle Pacific, which reduces the averaged high cloud amounts in the whole regions compared those around maritime continents (c.f., Figures 1 and 2). Furthermore, minimal seasonal changes in high clouds within these deep convection areas are found owing to persistent preferred convergence conditions throughout the analyzed normal years. Although extreme climate events could be good opportunities in testing models, the normal climate conditions characterized here should provide a baseline for parameterizing the clouds in GCMs.

Histograms of the bulk ice/liquid water paths for the high and low clouds in the selected areas are shown in Figures 5 and 6, respectively, for June, July and August (JJA, left column) and December, January, and February (DJF, right column) for 2003 (black), 2004 (red), and 2005 (green). The numbers listed in these figures are the means (left column) and standard deviations (right column) of the distributions. To properly display the statistically-significant

characteristics of IWP and LWP distributions, only water path values less than 300 gm^{-2} are plotted. For each type of clouds in a given area, the ice and liquid water amount ranges are extremely broad, from close to zero to well above 5,000 gm^{-2} (c.f. Lin and Rossow 1997). The frequencies for precipitating clouds with extreme high ice and liquid water paths above 1,000 gm^{-2} in individual statistical bins (or intervals) are extreme low and not statistically stable (Lin and Rossow 1997). Actually, even for IWP or LWP at values close to 300 gm^{-2} the frequencies are already near zero as indicated in the figures. Because of their rare occurrence the clouds with these extreme IWP and LWP values contribute little to the radiation forcing and budget of their type of clouds although they may influence atmospheric hydrology and precipitation significantly. Because the currently available MODIS retrievals for precipitating clouds are limited to optical depths $\leq$ 128 (Minnis *et al.* 1995), the IWP or LWP values are probably underestimated for extremely thick clouds. The extremely high IWP and LWP values obtained by Lin and Rossow (1994, 1997) were estimated from satellite passive microwave measurements that are not available for this study. To avoid misleading the statistics of IWP or LWP values due to extreme cases, the values higher than 1,000 gm^{-2} are not included in the mean and standard deviation calculations in current study. Because of dramatic variations (or chaotic characteristics of) in storm systems from rainfall cells to extended stratiform anvils and thin cirrus clouds, the standard deviations of the analyzed high clouds are generally much bigger than their corresponding averages (Figure 5) even without the extreme IWP and LWP values. The IWP distributions of these storms skew towards small IWP values with peaks around 10 gm^{-2}. Very high frequencies of high cirrus and cirrostratus clouds dominate the radiation fields of these storm cloud systems. As expected, mid-latitude winter storms contain more ice than those during summer seasons. Generally, mid-latitude storms have larger seasonal variations than the tropical systems. For example, the average IWP values for the North Atlantic storm tracks change from about 37 gm^{-2} to around 80 gm^{-2} during summer and winter seasons, respectively, while the maximum seasonal IWP differences for tropical high clouds are ~15 gm^{-2}, mostly within 10 gm^{-2}. The seasonal changes in large-scale dynamics, sea surface temperatures, and atmospheric temperature and humidity structures are much greater in mid-latitudes compared to those in the tropics.

For low clouds (Figure 6), the mean values are relatively high and vary from ~55 gm^{-2} to 70 gm^{-2} for all selected areas in both summer and winter seasons. Compared with summer

values, the winter LWP means may be slightly greater, likely due to reduced relative humidity in the boundary layer during warm months as reported in previous observations and analyses of low cloud variations with temperature (e.g., Tselioudis *et al.* 1992, Del Genio and Wolf 2000, Lin *et al.* 2003). The LWP distributions for individual areas in a specific season have much higher cumulated probabilities around their peak occurring frequencies and means compared to those of high stormy clouds, which results in relatively smaller standard deviations about 2/3 of their corresponding means.

Of all clouds observed, the inter-annual variabilities of these clouds are much smaller than the seasonal variabilities. The high clouds from the North Atlantic storm tracks show the greatest variability with the changes in ice water path of about 50 and 10 gm^{-2} seasonally and interannually, respectively.

The huge variability of individual cloud systems for all of the analyzed clouds poses a great challenge for cloud modeling. However, Figures 5 and 6 show that the probability distributions of condensed water for a given cloud type change very little from year to year in each selected area. The shapes, means, and standard deviations of the same type of clouds from different areas are also very similar. These results demonstrate that the cloud characteristics may vary drastically from one individual cloud system to another. But the overall characteristics of the same cloud types in normal conditions (in other words, forced by similar large-scale dynamics and thermodynamics) are very stable. It is over monthly or longer temporal scales in certain areas that stable statistics of cloud properties for the same type of clouds are obtained and can be meaningfully simulated by models.

The monthly mean TOA net radiative fluxes for clouds in the storm track and stratus deck regions are shown in Figure 7. These values, for the most part, represent the amount of radiation that is gained or lost in the Earth-atmosphere system below cloud top. The high clouds associated with mid-latitude storms (upper panel) are generally thick and reflect significant amounts of solar radiation. During the winter seasons, when solar radiation at these latitudes is weak, there is little shortwave irradiance passing into the atmosphere through the clouds, and the net radiation, a combination of minimal shortwave heating and considerable longwave cooling, thus, becomes negative. This cooling effect can be very strong and drops to as low as about -100 Wm^{-2}. When the insolation is greatest (or summer months), the shortwave radiation can penetrate into the atmosphere through non-precipitating parts of the storm systems, providing

significant amounts of solar heating to the surface and troposphere. The stormy clouds also block most of the strong longwave radiation emitted to space by the warmer seas during summer. These combined shortwave and longwave effects during warm seasons generally heat the storm track areas, although the magnitude of the heating (> ~120 Wm^{-2}) is not as large as that in clear conditions or in marine-stratus areas (c.f. lower panel). There, the radiative fluxes in the stratus deck areas display similar but slightly stronger annual cycles compared to those in the storm tracks owing to the annual solar insolation cycle and the strong seasonal cloud variations (Figure 3). A difference between the subtropical low clouds and storm-track high clouds is that in the stratus regions, the net radiation warms the Earth-atmosphere system all year, primarily in the boundary layer and the sea surface (c.f., discussions of Figure 10 below). This year-round warming is a result of greater insolation during winter in these areas compared to that in the mid-latitudes. Although the averaged net radiation for both the mid-latitude storm system and stratus cloud areas is positive (or heating), the cloud radiative forcing, defined as the net radiation difference between all-sky and clear-sky conditions, is negative. That is, the clouds actually cool the atmosphere relative to clear skies because the amount of solar radiation reflected back to space is much greater in cloudy conditions (not shown).

The TOA net radiation for the high clouds in tropical convergence zones (upper panel of Figure 8) varies much less (~100 Wm^{-2}) than that in the subtropics and mid-latitudes primarily because of smaller insolation variations. Small changes in sea surface temperature and the atmospheric temperature and humidity profiles around equatorial regions also minimize the radiation variability. Although tropical convective regions (lower panel), such as the Indian Ocean (red), TWP (green), and ITCZ (black) have even less seasonal variability than individual convection areas, the double peaks of the radiation fields in each annual cycle can be found clearly, especially for those in the ITCZ. Even though cold deep convective systems dominate tropical reflection of shortwave energy and release very little thermal radiation to space, more than half of the solar radiation still manages to enter the troposphere (Lin *et al.* 2002, 2006). Thus, the semi-annual equator crossing of the sun leaves a significant signature in the observed radiation records of the high clouds along ITCZ areas.

To further evaluate the similarities and differences of cloud radiation among the same types of clouds from different areas, we artificially shift the TOA net radiation forward 6 months periodically for clouds in the Northern Hemisphere. Figure 9 reveals very consistent annual

variations in both the phase and amplitude (250 - 300 Wm^{-2}) of the monthly mean net radiative fluxes from all of the different storm track areas (upper panel) and from all of the stratus regions (lower panel). Even though there are some latitudinal differences (i.e., difference in insolation) among them, the overlap of the averaged radiative fluxes for the analyzed storm track regions is so tight that it confirms certain inherit cloud-type features, such as similar ice water amount and variability of these clouds (c.f. Figure 5). As mentioned previously, although extreme precipitating clouds are important for upper-tropospheric moisture transport, cirrus and anvil formation, and climate hydrology (Lin *et al.* 2006) and may not have a stable statistic in an area for an individual month, such clouds are so rare that they do not significantly alter the basic radiative statistics for this cloud type. It is the normal clouds that dominate the radiation statistics because of their large spatial extent (and/or high frequency).

Compared to the mid-latitude storm clouds, the stratus cloud decks (Figure 9, lower panel) generally have similar annual oscillations in their net radiation averages, although these averages (or the net radiative energy into the atmosphere is) are higher because the solar insolation is stronger for these lower latitude clouds. The area off Australia's west coast shows the biggest annual changes in the net radiative fluxes (red) into the Earth's climate system among the four selected stratus deck areas. The largest annual amplitude for the clouds in the area probably is caused by having the highest LWP contrasts between the winter and summer seasons (the differences slightly exceed 10 gm^{-2}, c.f. Figure 6).

Overall, for all of the cloud types, the inter-hemispheric radiation differences between clouds from northern and southern hemispheres are minimal (c.f. Figures 8 and 9). It seems that the differences in dynamics and thermodynamics among the various regions and cloud types have significant impacts on the seasonal changes in cloud cover, but appear to affect cloud water content and, hence, radiation only secondarily. From a climate perspective, then, cloud cover is the component that will most affect or be affected by changes in the climate system. That is, changes in the radiation fields will depend mostly on changes in cloud amount in a given region for a particular cloud type. This result, along with the observed IWP and LWP values of these types of clouds (c.f. Figures 5 and 6), provides an effective tool for models to test their cloud simulation schemes from instantaneous to monthly or longer temporal scales in these typical cloud regimes.

The time series of the surface net radiation for the selected typical areas (Figure 10) have similar seasonal and interannual patterns as those at TOA except with greater magnitudes. The larger positive heating at the surface compared to that at TOA is an indicator of the greenhouse effect of the atmosphere and these clouds. Currently the variation (actually the feedback) of this cloud greenhouse effect with direct atmospheric greenhouse warming is not well documented. It is critical to analyze the greenhouse effect in

(Kondratyev and Varotsos 1995). The hemispherically normalized seasonal surface radiation values from different storm track regions (Figure 10, upper panel) follow each other closely reflecting the similarities in shortwave reflection at the TOA and surface, sea surface temperature, and boundary-layer temperature and humidity. Slightly lower net surface radiation for the clouds off the west coast of Australia during winter months compared to those of other stratus deck areas (Figure 10, lower panel) may result from its higher LWP values (c.f. Figure 6). The surface radiation in the ITCZ and SPCZ regions (Figure 11) has almost the same features as those seen for the other cloud types and at the TOA except with much smaller variability. The double peaks in the surface radiation time series for each annual cycle can still be seen in this figure although they are not as pronounced as those of the TOA net radiation fluxes. Very small variations in surface temperature as well as the thermal and moisture structures of the tropical atmosphere with annual cycle reduce interseasonal surface radiation changes, especially for longwave.

Time series of the monthly mean IWP and LWP, including extreme values during studied periods, are shown in Figures 12 and 13 for the selected high and low cloud areas, respectively. Because of extremely high IWP and LWP values in very few precipitating clouds (Lin and Rossow 1994, 1997), the overall means are slightly higher than the values shown in the histogram plots (c.f. Figures. 5 and 6), especially for storm-track cases. For low clouds, the differences are small due to very infrequent precipitation of this type of regime. The averaged IWP values (about 80 gm^{-2}) in the storm tracks (Figure 12, top panel) are generally higher than those (about 50 gm^{-2}) in tropical convergence zones (Figure 12, middle and bottom panels) due to more thin cirrus clouds in tropical convective systems than in the mid-latitude storms. The current satellite mean IWP retrievals generally agree very well with previous IWP estimates obtained from combined satellite visible, infrared and microwave measurements when the

uncertainties in the previous estimates are considered (Lin and Rossow 1994, 1996). As noted earlier, they also agree well with those determined from the CloudSat cloud radar (Waliser *et al.*, 2009). The IWP values for the North Pacific storm track (upper panel, green curve) have the largest seasonal cycles varying from 130 gm^{-2} during winter months to 60 gm^{-2} in summer months. The IWP over the North Atlantic storm track is noisier than its North Pacific counterpart. These small time scale variations may also cause a larger interannual change compared to those in other storm track areas and tropical convergence zones (also c.f., Figure 5). As mentioned previously, the IWP estimates for tropical high clouds vary minimally during these 3 normal years, especially for the combined tropical and ITCZ regions (Figure 12, bottom panel).

The LWP values for the stratus clouds from different areas (Figure 13) are around 60 gm^{-2} and exhibit similar seasonal and interannual variations, as shown in the analysis of the histograms in Figure 6. These *Aqua* LWP retrievals are very consistent with our previous combined satellite visible, infrared and microwave measurements (Lin and Rossow 1994, 1996, Lin *et al*. 1998, Ho *et al.* 2003), suggesting that the techniques for satellite LWP retrievals are generally mature enough for operational or long-term cloud monitoring.

4. Summary and conclusions

This study uses *Aqua* visible and infrared narrow- and broad-band measurements of the CERES and MODIS to evaluate the similarities in and differences of cloud radiation and liquid and ice water paths among the same types of clouds. Typical high clouds such as those found in the mid-latitude storm tracks and tropical convergence zones are considered. The subtropical stratus cloud decks off the west coasts of major continents were selected to represent low clouds. Generally, the same types of clouds from different areas exhibit significantly different time series of radiative fluxes due mainly to the differences in solar insolation and local atmospheric profiles. When these clouds are analyzed by accounting for the inter-hemispherical seasonal differences, the discrepancies in the radiative fluxes are remarkably diminished. As expected, the variabilities of individual storms and solid stratus cloud decks are significant: the standard deviations of LWP and IWP values are generally comparable to or even larger than the means for these cloud systems. Although the LWP or IWP distributions of these clouds can exceed the retrieval upper limits, the occurrence frequencies of these extreme satellite pixels are rare. The statistical distributions of water amounts at normal range (0 ~ 1000 gm^{-2}) are very stable for

different periods and areas. These results comprise a set of valuable observations for testing modeled cloud statistics and for improving cloud model parameterizations. Because of the stable statistical characteristics of cloud water amount and radiation, there is great potential for reducing the large uncertainties in modeled cloud radiative forcing. Future work will focus on the investigation of other cloud types such as marine cumulus, polar clouds, and clouds over land areas and on the influence of these clouds on the atmospheric hydrological cycle.

Acknowledgement

The authors would like to express their appreciation to B. Wielicki, G. Gibson, K.-M. Xu, D. Young, and D. Garber for their invaluable comments and suggestions. This research was supported by NASA's CERES mission and the NASA Energy and Water cycle Studies (NEWS) program. The CERES products were obtained from the NASA Langley Atmospheric Sciences Data Center in Hampton, Virginia.

References

BARKSTROM, B., HARRISON, E., SMITH, G., GREEN, R., KIBLER, J. AND CESS, R., 1989, The Earth Radiation Budget Experiment (ERBE) archival and April 1985 results, *Bulletin of American Meteorological Society*, **70**, pp. 1254-1262.

BONY, S., et al., 2006, How Well Do We Understand and Evaluate Climate Change Feedback Processes? *Journal of Climate*, **19**, pp. 3445–3482.

CESS, R., ZHANG, M., WIELICKI, B., YOUNG, D., ZHOU, X.-L. AND NIKITENKO, Y., 2001, The influence of the 1998 El Niño upon cloud-radiative forcing over the Pacific warm pool. *Journal of Climate*, **14, pp.** 2129-2137.

CHANG, F.-L. AND LI, Z., 2005a, A new method for detection of cirrus-overlapping-water clouds and determination of their optical properties, *Journal of Atmospheric Sciences*, **62**, pp. 3993-4009.

CHANG, F.-L. AND LI, Z., 2005b, A near-global climatology of single-layer and overlapped clouds and their optical properties retrieved from Terra/MODIS data using a new algorithm, *Journal of Climate*, **18**, pp. 4752-4771.

CHIRIACO, M., et al., 2007, Comparison of CALIPSO-like, LaRC, and MODIS retrievals of ice cloud properties over SIRTA in France and Florida during CRYSTAL-FACE, *Journal of Applied Meteorology and Climatology*, **46**, pp. 249-272.

DEL GENIO, A. AND WOLF, A., 2000, Climatic implications of the observed temperature dependence of the liquid water path of low clouds in the southern great plains, *Journal of Climate*,**13**, pp. 3465-3486.

DEL GENIO, A.D. AND KOVARI, W.,2002, Climatic properties of tropical precipitating convection under varying environmental conditions, *Journal of Climate*, **15**, pp. 2597-2615.

DEL GENIO, A.D., KOVARI, W., YAO, M.-S., AND JONAS, J., 2005, Cumulus microphysics and climate sensitivity, *Journal of Climate*, **18**, pp. 2376-2387.

DONG, X., MINNIS, P., XI, B., SUN-MACK, S. AND CHEN, Y., 2008, Comparison of CERES-MODIS stratus cloud properties with ground-based measurements at the DOE ARM Southern Great Plains site, *Journal of Geophysical Research*, **113**, D03204, doi:10.1029/2007JD008438.

EITZEN, Z., XU, K.-M. AND WONG, T., 2008, Statistical Analyses of Satellite Cloud Object Data from CERES. Part V: Relationships Between Physical Properties of Boundary-layer Clouds, *Journal of Climate*, **21**, pp. 6668–6688.

HARTMANN, D.L. AND MICHELSON, M.L., 1993, Large-scale effects on the regulation of tropical sea surface temperature, *Journal of Climate*, **6**, pp. 2049-2062.

HARTMANN, D.L. AND MICHELSON, M.L., 2002, No evidence for iris, *Bulletin of American Meteorological Society*, **83**, pp. 249-254.

HO, S.-P., LIN, B., MINNIS, P. AND FAN, T.-F., 2003, Estimation of cloud vertical structure and water amount over tropical oceans using VIRS and TMI data, *Journal of Geophysical Research*, **108** (D14), 4419, doi:10.1029/2002JD003298.

Jakob, C. and Tselioudis, G., 2003: Objective identification of cloud regimes in the Tropical Western Pacific, *Geophys. Res. Lett.*, **30**, issue 21, Article Number: 2082, doi:10.1029/2003GL018367.

JAKOB, C., TSELIOUDIS, G. AND HUME, T., 2005, The radiative, cloud, and thermodynamic properties of the major tropical western Pacific cloud regimes, *Journal of Climate*, **18** , pp. 1203-1215.

KLEIN, S. A. AND HARTMANN, D.L., 1993, The seasonal cycle of low stratiform clouds, *J. of Climate*, **6**, pp. 1587-1606.

KONDRATYEV, K.Y. AND VAROTSOS, C., 1995, Atmospheric greenhouse effect in the context of global climate change. *Nuovo Cimento della Societa Italiana di Fisica C-Geophysics and Space Physics*, **18**, pp. 123-151.

LIN, B. AND ROSSOW, W.B., 1994, Observations of cloud liquid water path over oceans: Optical and microwave remote sensing methods, *Journal of Geophysical Research*, **99**, pp. 20907-20927.

LIN, B. AND ROSSOW, W.B., 1996, Seasonal variation of liquid and ice water path in non-precipitating clouds over oceans, *Journal of Climate*, **9**, pp. 2890-2902.

LIN, B. AND ROSSOW, W.B., 1997, Precipitation water path and rainfall rate estimates over oceans using Special Sensor Microwave Imager and International Satellite Cloud Climatology Project data, *Journal of Geophysical Research*, **102**, pp. 9359-9374.

527 LIN, B., WIELICKI, B., MINNIS, P. AND ROSSOW, W.B,., 1998a, Estimation of water cloud
528 properties from satellite microwave, infrared, and visible measurements in oceanic
529 environments. I: Microwave brightness temperature simulations, *Journal of Geophysical*
530 *Research*, **103**, pp. 3873-3886.
531 LIN, B., MINNIS, P., WIELICKI, B., DOELLING, D.R., PALIKONDA, R., YOUNG, D.F. AND UTTAL, T,.,
532 1998b, Estimation of water cloud properties from satellite microwave, infrared, and visible
533 measurements in oceanic environments. II: Results, *Journal of Geophysical Research*, **103**,
534 pp. 3887-3905.
535 LIN, B., WIELICKI, B., CHAMBERS, L., HU, Y. AND XU, K.-M,., 2002, The Iris hypothesis: A
536 negative or positive cloud feedback? *Journal of Climate*, **15**, pp. 3-7.
537 LIN, B., MINNIS, P. AND FAN, A,., 2003, Cloud liquid water amount variations with temperature
538 observed during SHEBA experiment, *Journal of Geophysical Research*, **108** (D14), 4427,
539 doi:10.1029/2002JD002851.
540 LIN, B., WIELICKI, B., MINNIS, P., CHAMBERS, L., XU, K.-M., HU, Y. AND FAN, A,., 2006, The
541 effect of environmental conditions on tropical deep convective systems observed from the
542 TRMM satellite, *Journal of Climate*, **19**, pp.5745-5761.
543 LIN, B., XU, K.-M., MINNIS, P., WIELICKI, B., HU, Y., CHAMBERS, L., FAN, T. AND SUN, W., 2007,
544 Coincident occurrences of tropical individual cirrus clouds and deep convective systems
545 derived from TRMM observations, *Geophysical Research Letter*, **34**, L14804,
546 doi:10.1029/2007GL029768.
547 LIN, B., STACKHOUSE JR., P., MINNIS, P., WIELICKI, B., HU, Y., SUN, W., FAN, T. AND
548 HINKELMAN, L., 2008, Assessment of global annual atmospheric energy balance from satellite
549 observations, *Journal of Geophysical Research*, **113**, D16114, doi:10.1029/2008JD009869.
550 LINDZEN, R.S., CHOU, M.-D. AND HOU, A., 2001, Does the Earth have an adaptive infrared iris?
551 *Bulletin of American Meteorological Society*, **82**, pp. 417-432.
552 LUO, Z. AND ROSSOW, W., 2004, Characterizing tropical cirrus life cycle, evolution, and
553 interaction with upper-tropospheric water vapor using Lagrangian trajectory analysis of
554 satellite observations, *Journal of Climate*, **17**, pp. 4541-4563.
555 LUO, Y., XU, K.-M., WIELICKI, B., WONG, T. AND EITZEN, Z., 2007, Statistical analyses of
556 satellite cloud object data from CERES. Part III: Comparison with cloud-resolving model
557 simulations of tropical convective clouds. *Journal of Atmospheric Sciences*, **64**, pp. 762-785.

MACE, G. G., ZHANG, Y., PLATNICK, S., KING, M., MINNIS, P. AND YANG, P,., 2005, Evaluation of cirrus cloud properties from MODIS radiances using cloud properties derived from ground-based data collected at the ARM SGP site, *Journal of Applied Meteorology*, **44**, pp. 221-240.

MACHADO, L., ROSSOW, W., GUEDES, R. AND WALKER, A,., 1998, Life cycle variations of mesoscale convective systems over Americas, *Monthly Weather Review*, **126**, pp. 1630-1654.

MINNIS, P., 1995, Cloud Optical Property Retrieval (Subsystem 4.3). 'Clouds and the Earth's Radiant Energy System (CERES) Algorithm Theoretical Basis Document, Volume III: Cloud Analyses and Radiance Inversions (Subsystem 4)', NASA RP 1376**, 3**, pp. 135-176.

MINNIS, P., HUANG, J., LIN, B., YI, Y., ARDUINI, R., FAN, T., AYERS, J. AND MACE, G., 2007, Ice cloud properties in ice-over-water cloud systems using TRMM VIRS and TMI data, *Journal of Geophysical Research*, **112**, D06206, doi:10.1029/2006JD007626.

MINNIS, P., TREPTE, Q.Z., SUN-MACK, S., YAN CHEN, DOELLING, D.R., YOUNG, D.F., SPANGENBERG, D.A., MILLER, W.F., WIELICKI, B.A., BROWN, R.R., GIBSON, S.C. AND GEIER, E.B., 2008, Cloud detection in non-polar regions for CERES using TRMM VIRS and Terra and Aqua MODIS data, *IEEE Transaction on Geoscience and Remote Sensing*, **46**, pp. 3857 – 3884.

RAMANATHAN, V. AND COLLINS, W., 1991, Thermodynamic regulation of ocean warming by cirrus clouds deduced from observations of the 1987 El Nino, *Nature*, **351**, pp. 27-32.

RAPP, A., KUMMEROW, C., BERG, W. AND GRIFFITH, B., 2005, An evaluation of the proposed mechanism of the adaptive infrared iris hypothesis using TRMM VIRS and PR measurements, *Journal of Climate*, **18**, pp. 4185-4194.

REYNOLDS, R.W. AND SMITH, T., 1994, Improved global sea surface temperature analysis, *Journal of Climate*, **7**, pp. 929-948.

ROSSOW, W.B., TSELIOUDIS, G., POLAK, A. AND JAKOB, C., 2005, Tropical climate described as a distribution of weather states indicated by distinct mesoscale cloud property mixtures, *Geophys. Res. Lett*., **32**, issue 21, L21812, doi:10.1029/2005GL024584.

SU, H., READ, W., JIANG, J., WATERS, J., WU, D. AND FETZER, E,., 2006, Enhanced positive water vapor feedback associated with tropical deep convection: New evidence from Aura MLS, *Geophysical Research Letter*, **33**, L05709, doi:10.1029/2005GL025505.

SUN-MACK, S.,, MINNIS, P., CHEN, Y., GIBSON, S., YI, Y., TREPTE, Q., WIELICKI, B., KATO, S., WINKER, D., STEPHENS, G. AND PARTAIN, P., 2007, Integrated cloud-aerosol-radiation product

using CERES, MODIS, CALIPSO and CloudSat Data, SPIE Remote Sensing of Clouds and the Atmosphere XII, Proc. of SPIE, **6745**, , Florence, Italy, 17-19 September, 2007, edited by A. Comerón, R.H. Picard, K. Schäfer, J.R. Slusser, A. Amodeo, paper ID: 674513.

TSELIOUDIS, G., RIND, D. ANDROSSOW, W., 1992, Global patterns of cloud optical thickness variation with temperature, *Journal of Climate*, **5**, pp. 1642-1657.

WALISER, D., LI, F., WOODS, C., BACMEISTER, J., CHERN, J., DELGENIO, A., JIANG, J., KHARITONDOV, M., KUANG, Z., MENG, H., MINNIS, P., PLATNICK, S., ROSSOW, W., STEPHENS, G., SUN-MACK, S., TAO, W., TOMPKINS, A., VANE, D., WALKER, C. AND WU, D., 2009, Cloud ice: A climate model challenge with signs and expectations of progress. *Journal of Geophysical Research*, **114**, D00A21, doi:10.1029/2008JD010015.

WIELICKI, B., BARKSTROM, B., HARRISON,E., LEE, R., SMITH, G. AND COOPER, J., 1996, Clouds and the Earth's Radiant Energy System (CERES): An Earth observing system experiment, *Bulletin of American Meteorological Society*, **77**, pp. 853-868.

XU, K.-M., WONG, T., WIELICKI, B., PARKER, L. AND EITZEN, Z., 2005, Statistical analyses of cloud object data from CERES. Part I: Methodology and preliminary results of the 1998 El Niño/2000 La Niña. *Journal of Climate*, **18,** pp. 2497-2514.

XU, K.-M., WONG, T., WIELICKI, B., PARKER, L., LIN, B., EITZEN, Z. AND BRANSON, M., 2007, Statistical analyses of satellite cloud object data from CERES. Part II: Tropical convective cloud objects during 1998 El Niño and evidence for supporting the fixed anvil temperature hypothesis. *Journal of Climate*, **20**, pp. 819-842.

XU, K.-M., WONG, T., WIELICKI, B. AND PARKER, L., 2008, Statistical analyses of satellite cloud object data from CERES. Part IV: Boundary-layer cloud objects during 1998 El Niño. *Journal of Climate*, **21**, pp. 1500–1521.

ZHANG, M., LIN, W., KLEIN, S., BACMEISTER, J., BONY, S., CEDERWALL, R., DEL GENIO, A., HACK, J., LOEB, N., LOHMANN, U., MINNIS, P., MUSAT, I., PINCUS, R., STIER, P., SUAREZ, M., WEBB, M., WU, J.,. XIE, S., YAO, M. AND ZHANG, J, 2005, Comparing clouds and their seasonal variations in 10 atmospheric general circulation models with satellite measurements. *Journal of Geophysical Research*, **110**, doi:10.1029/2004JD005021.

Figure captions

Figure 1. Annual mean high (upper panel) and low (lower panel) cloud distributions from the CERES-MODIS cloud analysis of 2005 Aqua data.

Figure 2. Selected regions for stormy (upper panel) and stratus (lower panel) clouds. Individual colours and/or numerical labels represent individual cloud areas.

Figure 3. Time series of cloud cover (%) for storm track (upper) and stratus (lower) areas. Hereafter, all area numbers or labels indicated in the figures are consistent with those shown in Figure 2 and discussed in the text.

Figure 4. Similar as Figure 3, except for selected tropical areas (upper) and combined regions (lower).

Figure 5a. Histogram of IWP for high clouds in middle latitude storm tracks during June, July and August (JJA, left) and December, January, and February (DJF, right) for 2003 (black), 2004 (red), and 2005 (green). Means and standard deviations are listed in the left and right columns, respectively, in each plot.

Figure. 5b. Same as 5a, except for ITCZ areas.

Figure 6. Histogram of LWP for stratus clouds during June, July and August (JJA, left) and December, January, and February (DJF, right) for 2003 (black), 2004 (red), and 2005 (green).

Figure 7. Time series of TOA monthly mean net radiation (Wm^{-2}) for clouds in storm track (upper), and stratus (lower) areas.

Figure 8. Same as Figure 7, except for tropical convergence zones (upper) and their combined high cloud regions (lower).

Figure 9. TOA monthly mean net radiation (Wm^{-2}) for clouds in storm track (upper) and stratus (lower) areas. The Northern Hemisphere radiative fluxes are shifted forward 6 months to obtain the fluxes in the same seasons for all selected areas.

Figure 10. Same as Figure 9, except for surface (SFC) net radiation.

Figure 11. Same as Figure 8, except for surface (SFC) net radiation.

Figure 12. Time series of monthly mean IWP for high clouds in selected areas.

Figure 13. Time series of monthly mean LWP for low clouds in subtropical solid deck areas.

Figure 1. Annual mean high (upper panel) and low (lower panel) cloud distributions from the CERES-MODIS cloud analysis of 2005 Aqua data.

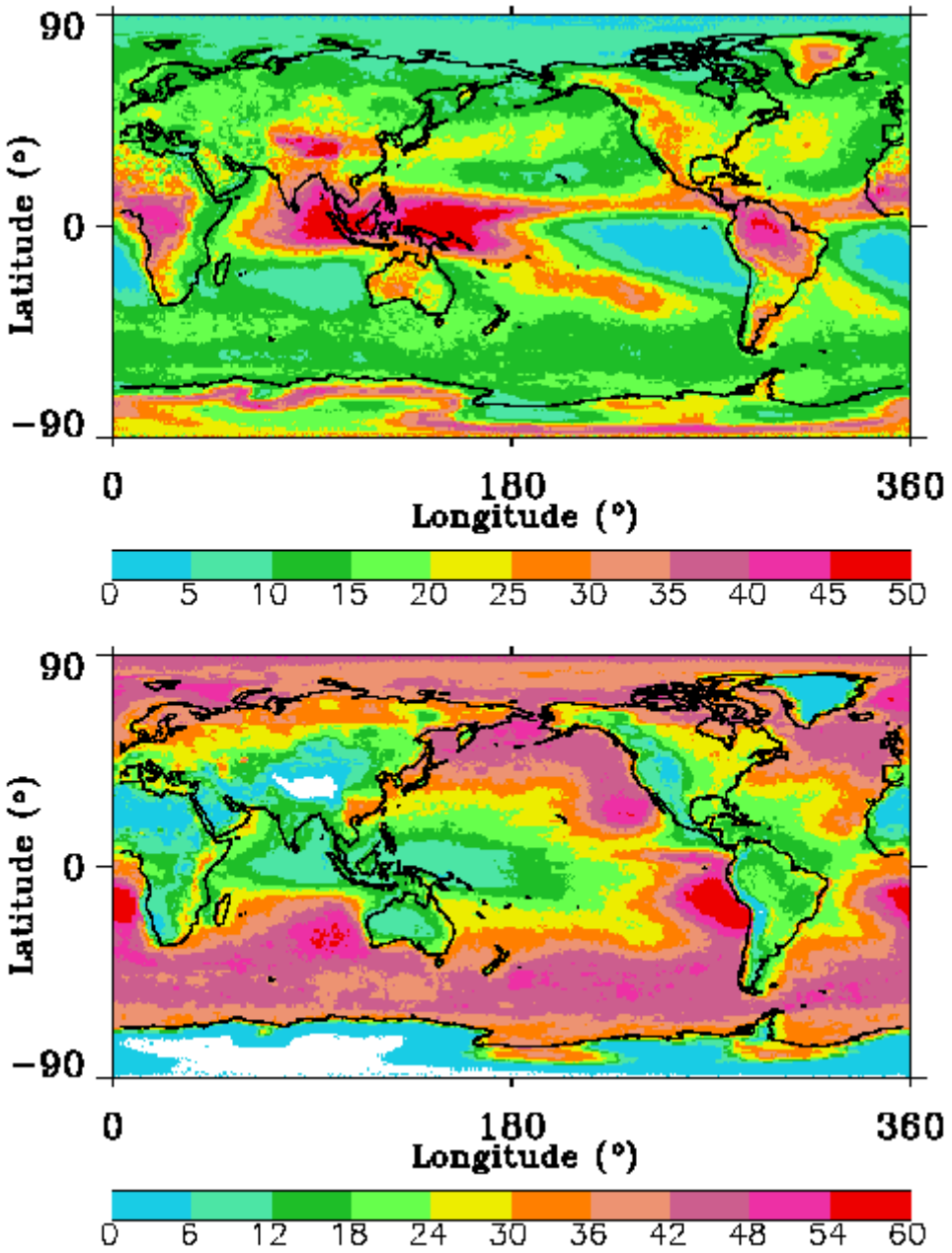

Figure 2. Selected regions for stormy (upper panel) and stratus (lower panel) clouds. Individual colours and/or numerical labels represent individual cloud areas.

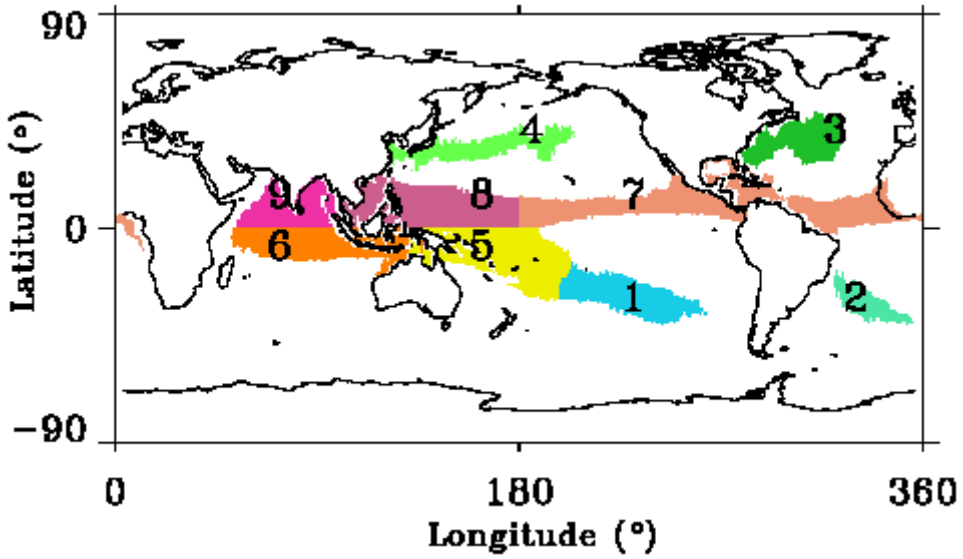

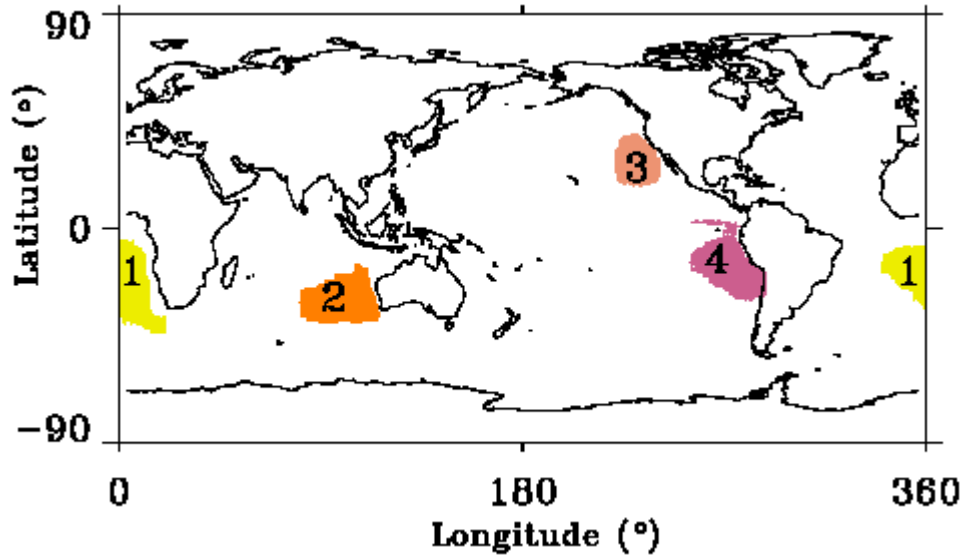

Figure 3. Time series of cloud cover (%) for storm track (upper) and stratus (lower) areas. Hereafter, all area numbers or labels indicated in the figures are consistent with those shown in Figure 2 and discussed in the text.

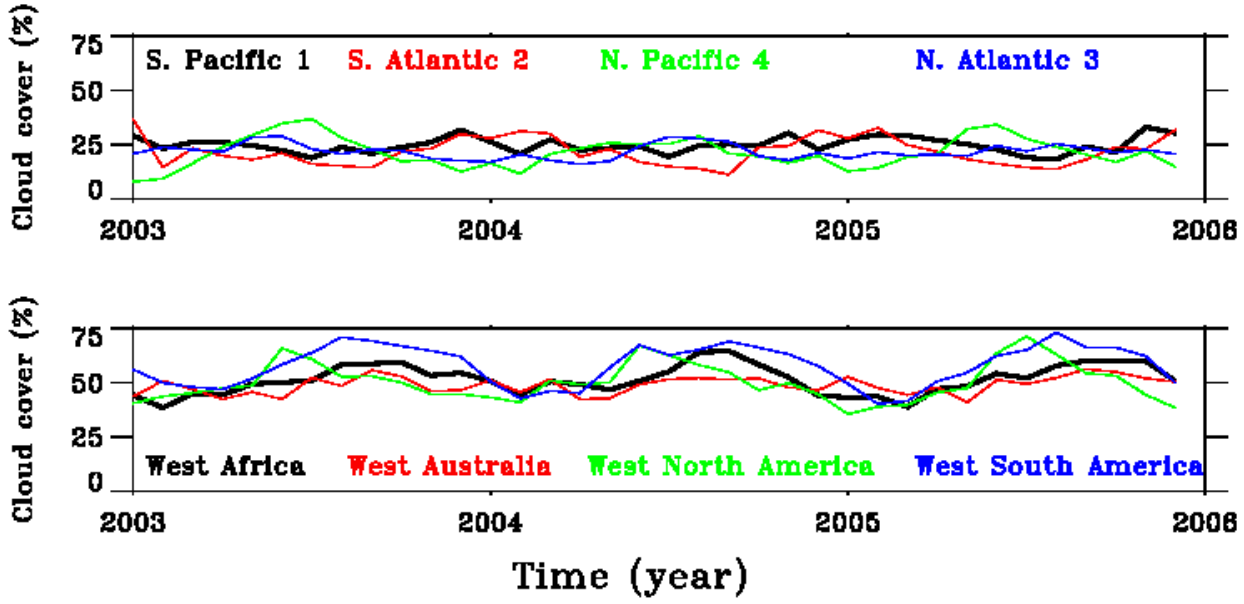

663 Figure 4. Similar as Figure 3, except for selected tropical areas (upper) and combined regions
664 (lower).

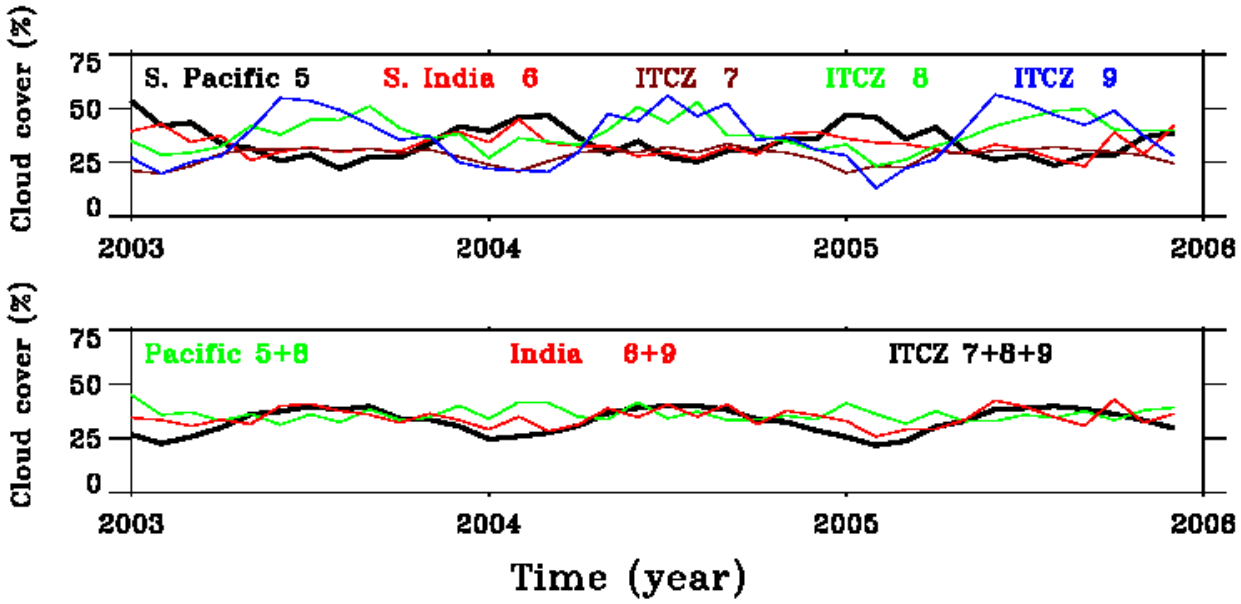

665

666

Figure 5a. Histogram of IWP for high clouds in middle latitude storm tracks during June, July and August (JJA, left) and December, January, and February (DJF, right) for 2003 (black), 2004 (red), and 2005 (green). Means and standard deviations are listed in the left and right columns, respectively, in each plot.

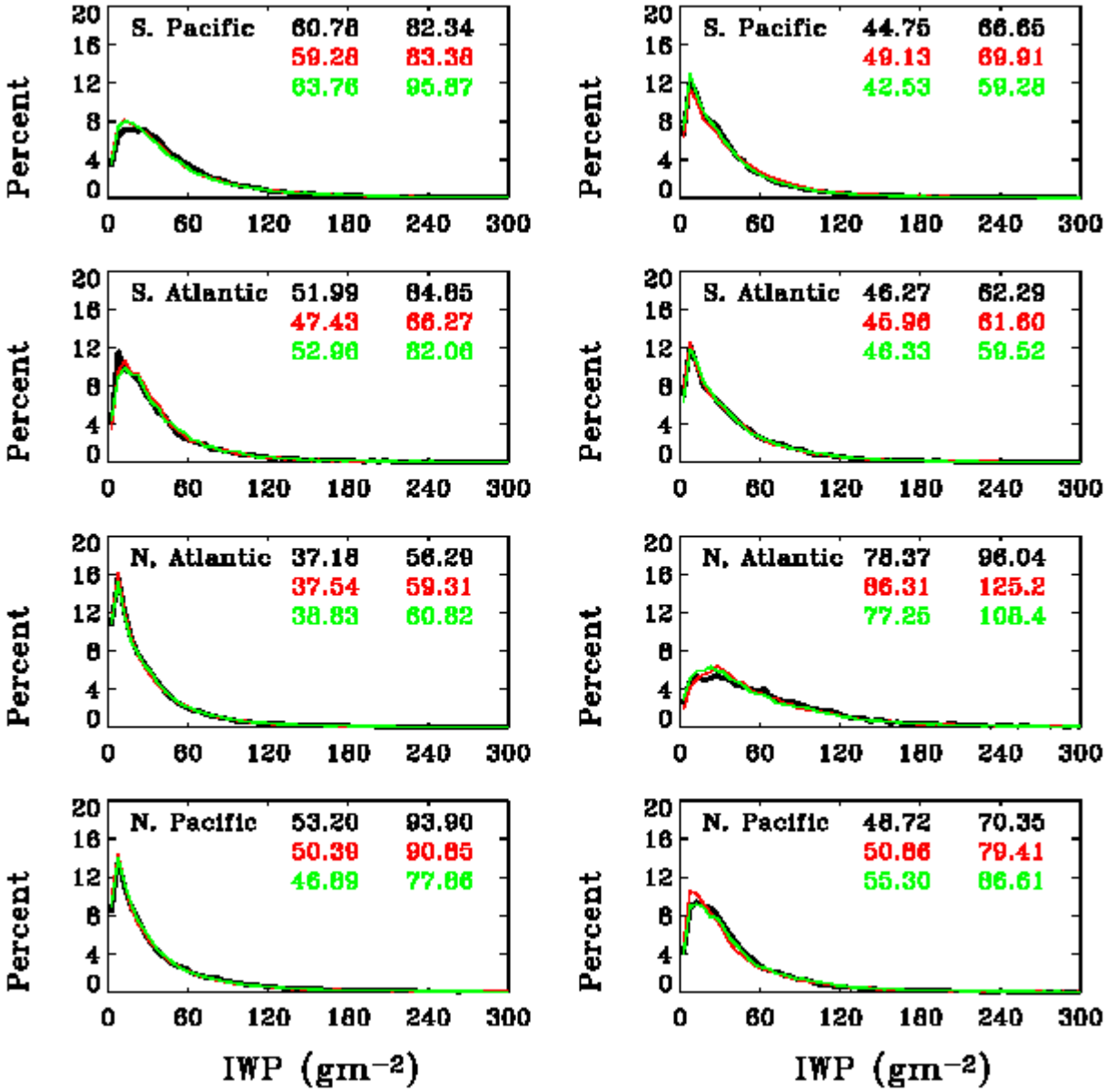

673 Figure 5b. Same as 5a, except for ITCZ areas.

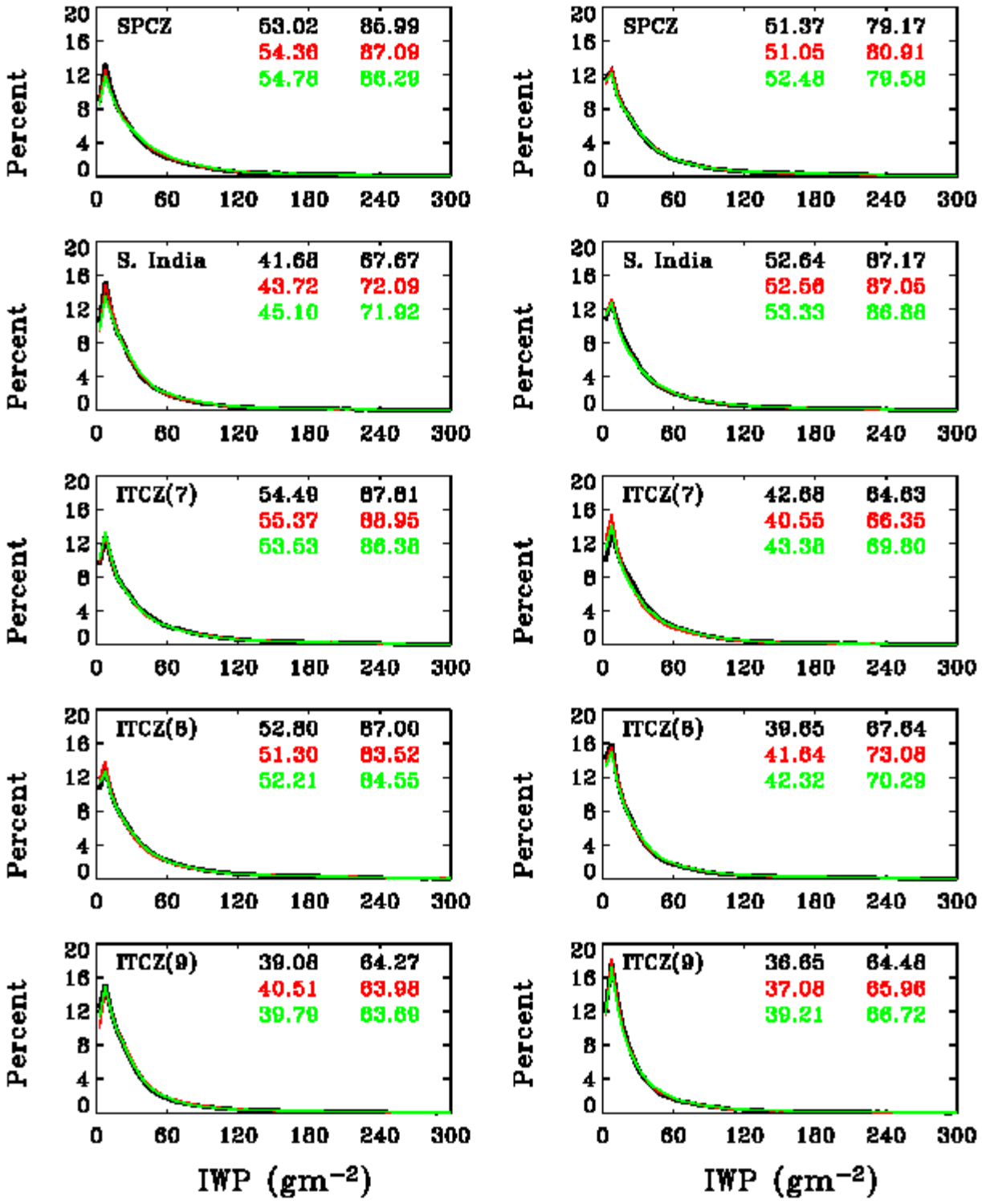

674

675

Figure 6. Histogram of LWP for stratus clouds during June, July and August (JJA, left) and December, January, and February (DJF, right) for 2003 (black), 2004 (red), and 2005 (green).

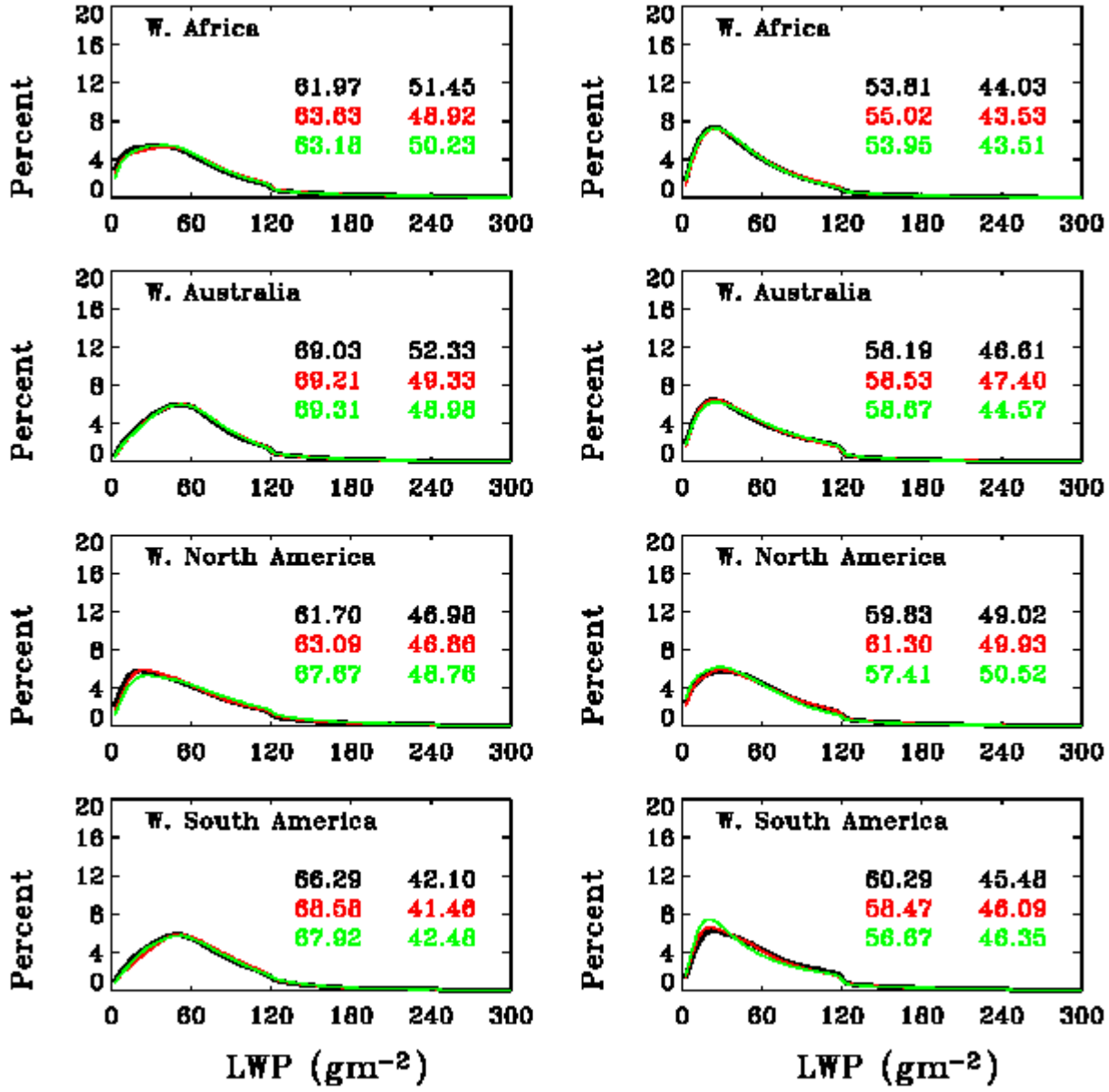

Figure 7. Time series of TOA monthly mean net radiation (Wm^{-2}) for clouds in storm track (upper), and stratus (lower) areas.

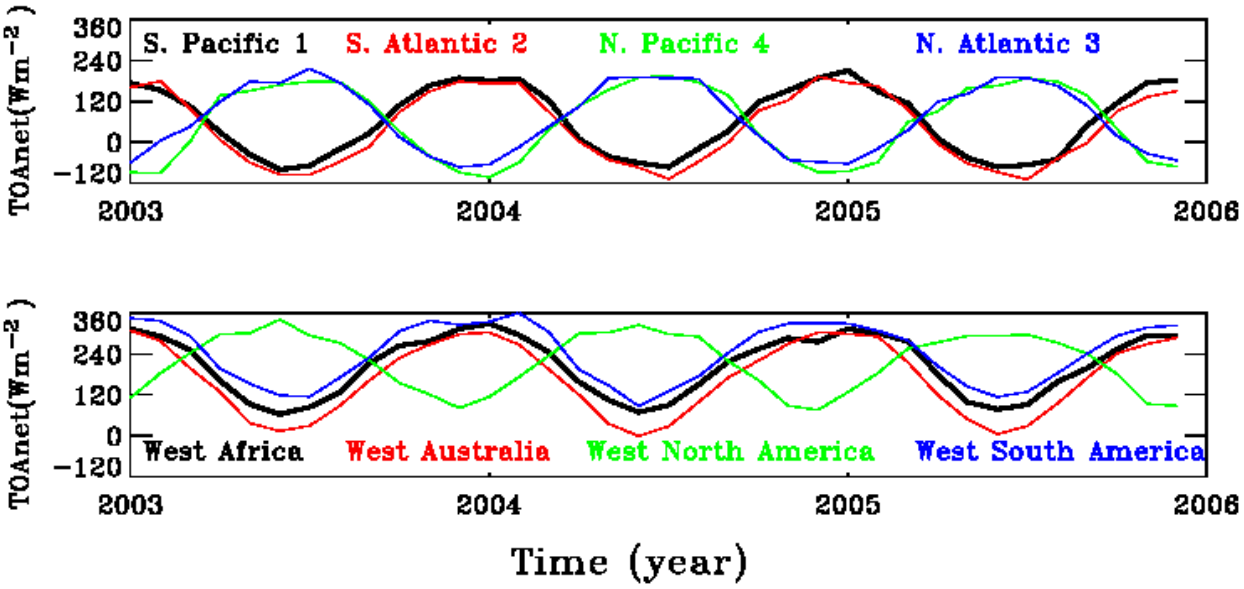

686 Figure 8. Same as Figure 7, except for tropical convergence zones (upper) and their combined
687 high cloud regions (lower).

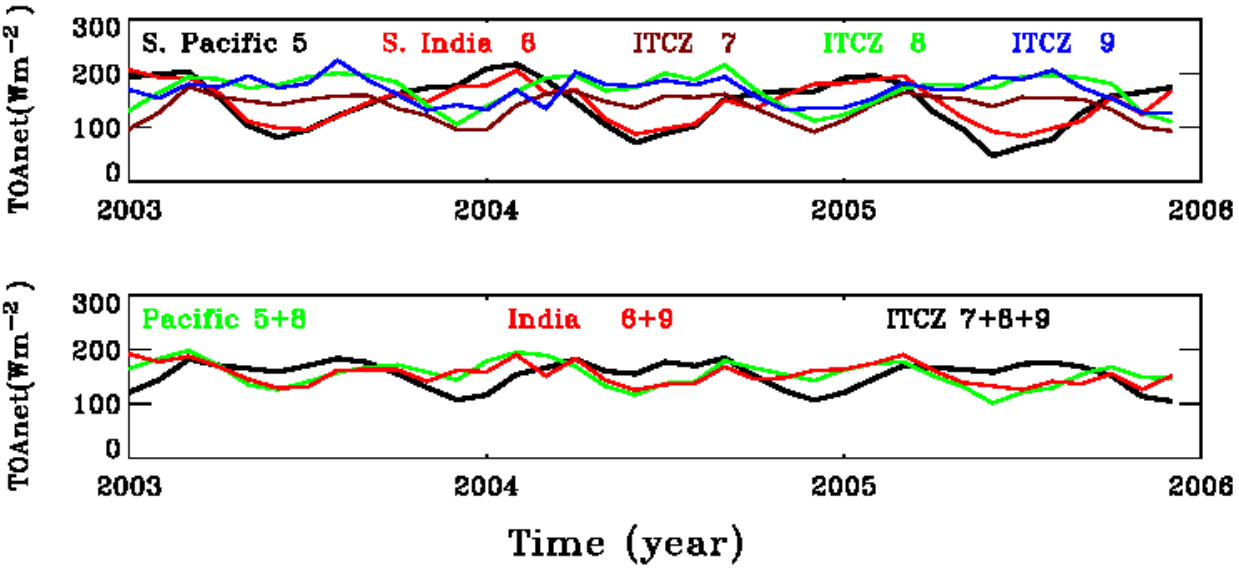

688

689

Figure 9. TOA monthly mean net radiation (Wm^{-2}) for clouds in storm track (upper) and stratus (lower) areas. The Northern Hemisphere radiative fluxes are shifted forward 6 months to obtain the fluxes in the same seasons for all selected areas.

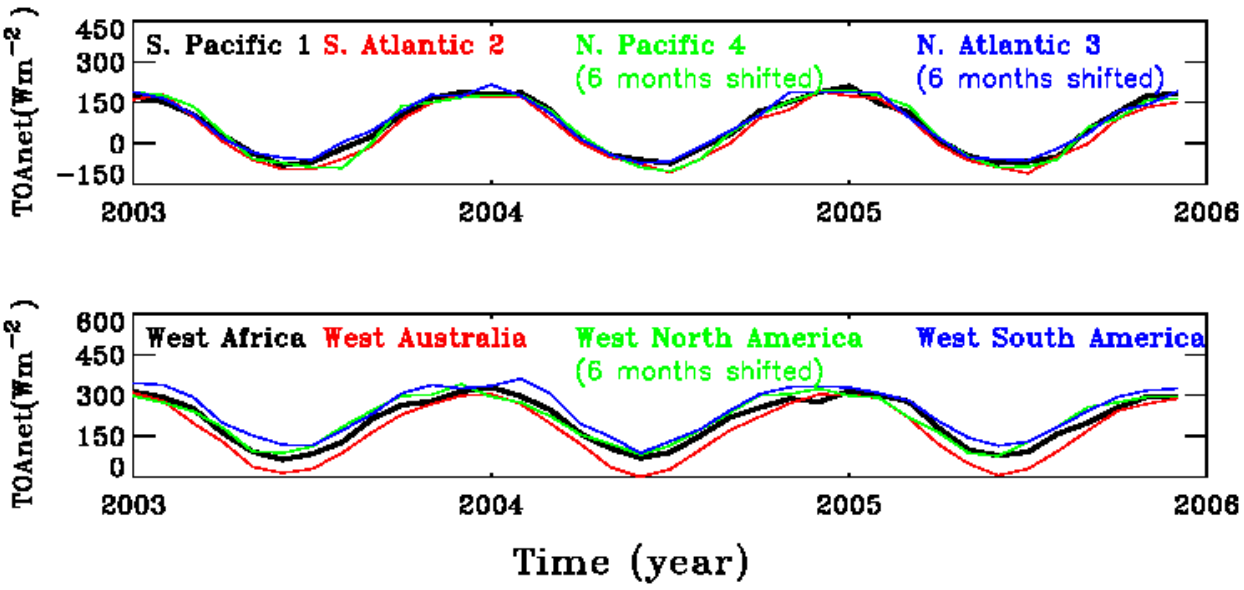

Figure 10. Same as Figure 9, except for surface (SFC) net radiation.

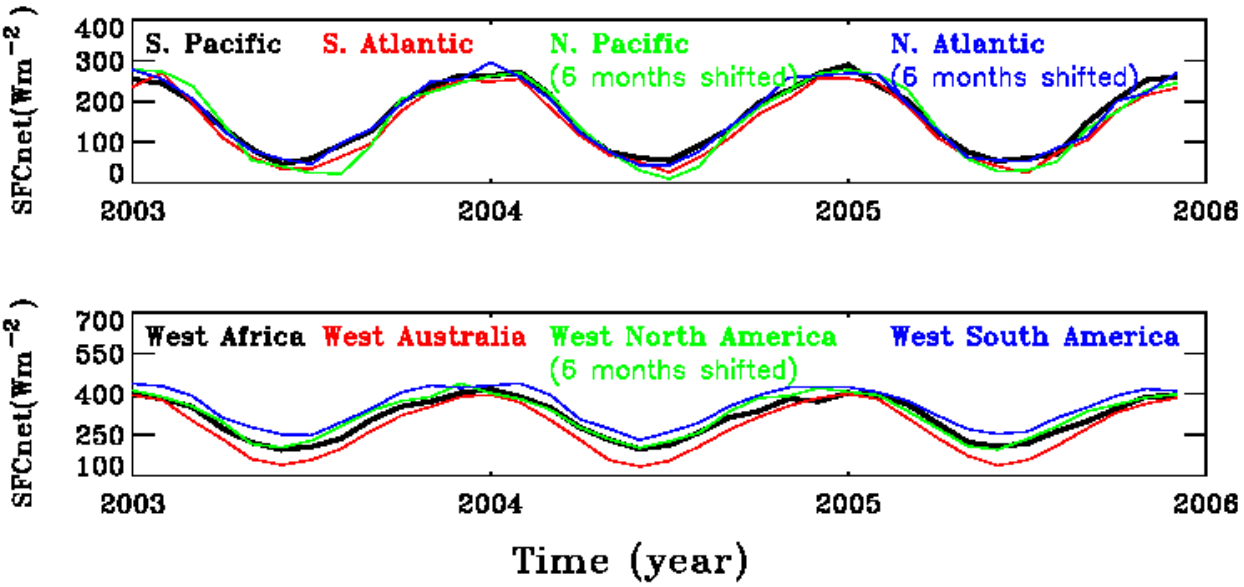

703 Figure 11. Same as Figure 8, except for surface (SFC) net radiation.

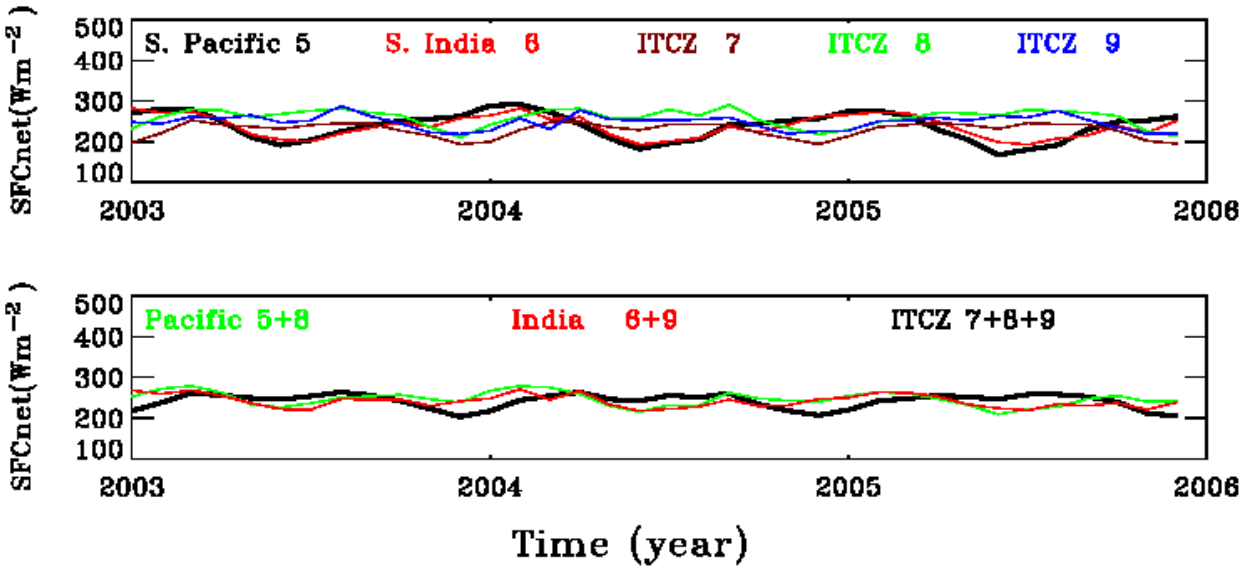

704

705

706

Figure 12. Time series of monthly mean IWP for high clouds in selected areas.

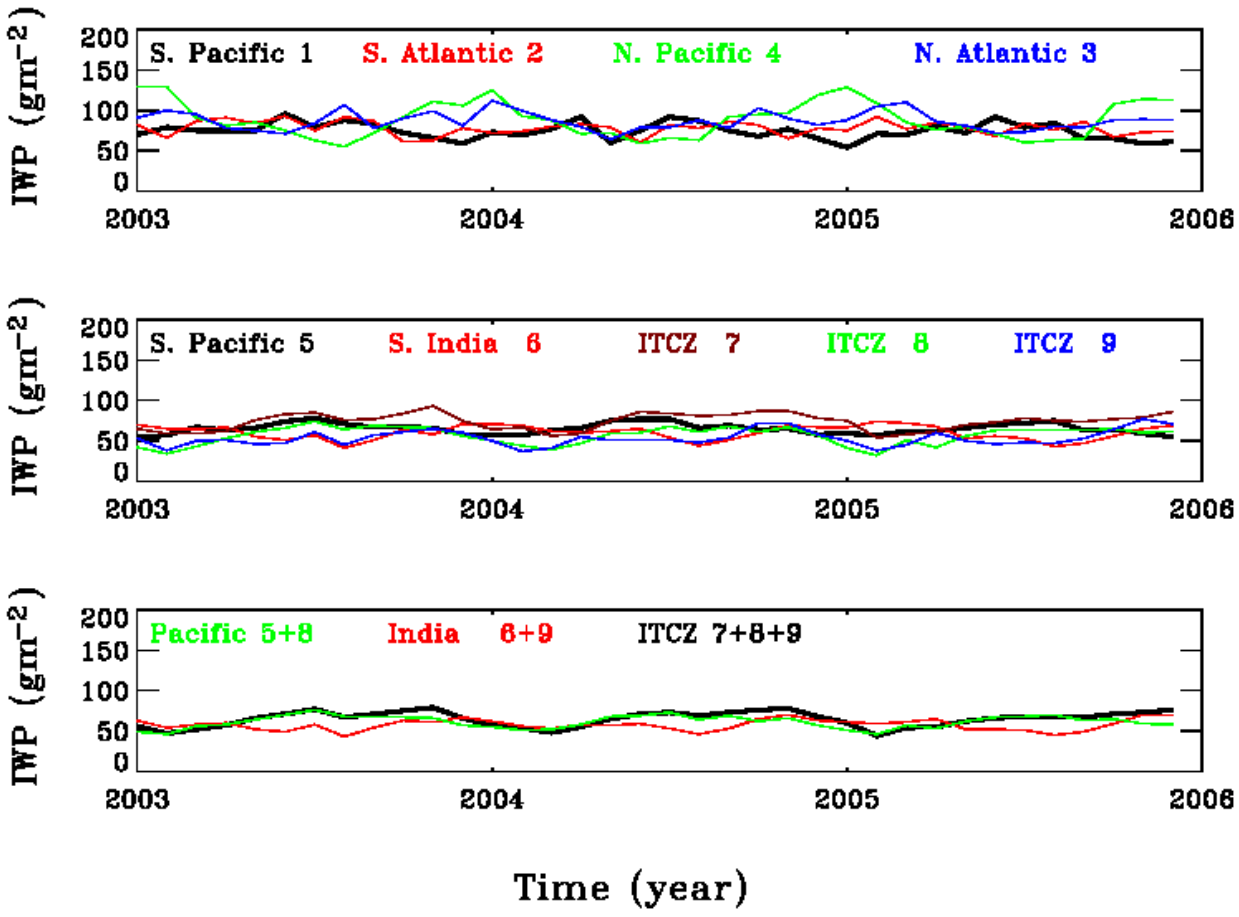

712 Figure 13. Time series of monthly mean LWP for low clouds in subtropical solid deck areas.

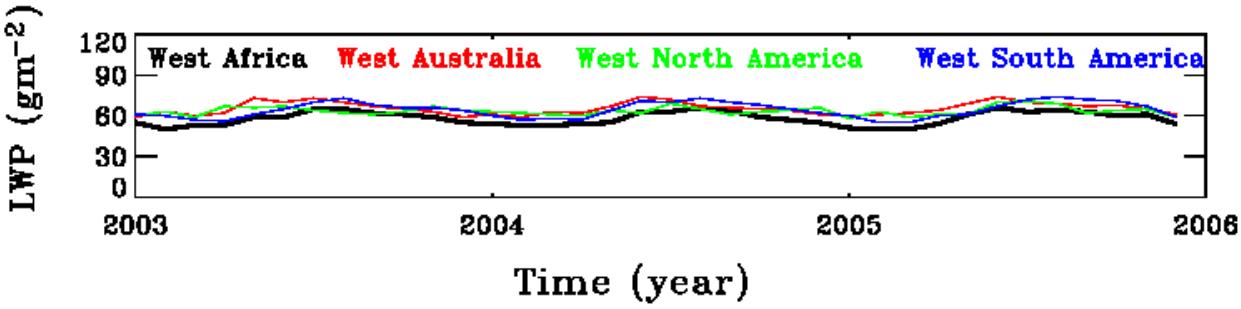

713

714

715

716